Preparation of Mineral Source Water From Deep Sea Water: Reduction of Sulfate Ion Using Selemion ASV Membrane

Hsiang-Yung Lu
Dept. of Chemical and Materials Engineering, National Ilan University, Yilan City, Yilan County 260, Taiwan, ROC

Chih-Shan Lin, Shih-Chi Lee, and Ming-Hong Ku
Stone & Resource Industry R&D Center, Ji'an Township, Hualien County 973, Taiwan, ROC

Jyh-Ping Hsu
Dept. of Chemical Engineering, National Taiwan University, Taipei City 106, Taiwan, ROC

Shiojenn Tseng
Dept. of Mathematics, Tamkang University, Danshui Township, Taipei County 251, Taiwan, ROC

Sung-Hwa Lin
Dept. of Chemical and Materials Engineering, National Ilan University, Yilan City, Yilan County 260, Taiwan, ROC

DOI 10.1002/aic.12319
Published online July 13, 2010 in Wiley Online Library (wileyonlinelibrary.com).

Adopting a laboratory-scaled electrodialysis (ED) process, we investigate the performance of a monovalent anion exchange permselective membrane in the reduction of the concentration of sulfate ions during the production of mineral source water from deep sea water (DSW). The dependence of the separation efficiency of anions on the operating time and the applied DC voltage is investigated based on a brine having salinity of about 15% prepared from DSW. The experimental results reveal that if the applied DC voltage is high, the change in the liquid volume during ED is dominated by the ions transported and the effect of electroosmosis. In addition, the amount of chloride ions transported correlates roughly linearly with the operating time, and the transport of sulfate ions is found to be blocked by chloride ions, presumably because of that the pore size of the permselective layer is close to the size of sulfate ions.
 AIChE J, 57: 1033–1042, 2011
Keywords: potable mineral water, deep sea water, electrodialysis, monovalent anion permselective membrane

Introduction

Producing adjustable potable mineral water from deep sea water (DSW) becomes more and more prevailing recently because the latter is characterized by being pure, free of land pollutants, and rich in vital mineral ions, such as magnesium and calcium. Its application, however, is limited considerably by the high concentration of sulfate ions in DSW. This problem may be solvable through adopting a membrane separation process. Functional membranes have been used widely in water treatments since 1970's. Although membrane is used widely for separating particulate materials from liquid

Correspondence concerning this article should be addressed to S.-H. Lin at shlin@niu.edu.tw.

Table 1. Typical Concentrations of the Main Ionic Species in DSW, RO Concentrated Brine, and LTVC Concentrated Brine

	Cations (mg/L)				Anions (mg/L)	
	Na^+	K^+	Ca^{2+}	Mg^{2+}	Cl^-	SO_4^{2-}
DSW	11800	439	434	1430	19200	2710
RO concentrated brine	17700	622	649	2140	28800	3890
LTVC concentrated brine	30190	1504	1355	5203	90226	10327

dispersion, membrane operations are more and more applied also for the removal of dissolved salts. Recent advances in fabrication techniques making it possible for membranes to be used in more advanced operations, such as ultrafiltration (UF), nanofiltration (NF), reverse osmosis (RO), ion-exchange, and ion-selection. Functional membranes are often adopted for purification of domestically used water, edible-salt production, and desalination of seawater and saline water. Ion-selective membrane is used widely in the electrodialysis process (ED) for water purification, industrial water treatment, edible-salt production, and adjustable mineral water production from sea water. In these applications, developing monovalent ion permselective membrane has become one of the key issues recently.[1–6] This type of membrane is capable of imposing appreciably different resistances on ions of various valences and sizes, yielding various permeabilities. The improvement in the properties of ion-selective membrane facilitates fast development in the production of both edible-salt and mineral water from sea water for the ion contents in the products, such as Na^+, K^+, Ca^{2+}, Mg^{2+}, and other valuable ions can be adjusted finely. Similarly, the contents of toxic ions and other undesired ions, such as SO_4^{2-}, can be reduced significantly through using monovalent ion permselective membrane. In practice, monovalent ion permselective membrane is prepared by coating a thin permselective polymeric layer on the surface of a regular ion-selective membrane. The permselective layer functions mainly by steric-repulsion or electric-repulsion mechanisms. The former is achieved by coating a highly cross-linked resin layer (for monovalent anion permselective membrane) and the latter by coating a polymer layer having charge of opposite sign to that of the ion-selective membrane (for monovalent cation permselective membrane).[1,2] Depending upon the sizes and the valences of ionic species, those two mechanisms yield barriers of various levels for ion transfer.

The transport of ionic species across the ion-selective membrane in ED involves their transfer through four regions, namely, the boundary layers near the membrane-liquid interfaces, the permselective layer (for monovalent ion permselective membrane), and the nonpermselective layer. Many theoretical and experimental attempts have been made in the literature on the description of the ionic transfer in ED and several models and/or effects are proposed, such as pseudo homogeneously structured membrane,[2,7–9] concentration polarization inside the boundary layer,[10–13] and heterogeneous surface layer.[1,2,14] These studies suggest that the transport of ionic species through a monovalent ion permselective membrane can be complicated. The possible presence of the effect of electroosmosis (the movement of liquid driven by the drag coming from ions) and that of osmosis (that driven by the concentration difference on the two sides of the membrane) makes it even more complicated. These effects are often ignored in previous studies.

Highly concentrated brine (RO concentrated brine) is usually used commercially as the raw liquid to produce potable mineral source water from DSW through UF and RO processes. Unfortunately, the high concentration of SO_4^{2-} in DSW (and the derived concentrated brine) limits its applications considerably, especially for potable purposes, and relevant information about the reduction of SO_4^{2-} is very limited. The functions of monovalent anion permselective membrane suggest that this problem might be solved by adopting it in ED. In this work, the potential usage of a commercial monovalent anion permselective membrane, Selemion ASV anion-exchange membrane (Asahi Glass Engineering), to reduce the concentration of SO_4^{2-} through a laboratory-scaled ED (CH-O type electrodialyzer, Asahi Glass Engineering) for the production of mineral source water is investigated. Concentrated brine prepared from RO concentrated brine using a low temperature vacuum concentrator (LTVC) is adopted as the raw material liquid. Here, we focus on the dependence of the separation efficiency of anions on the processing time and the applied direct current voltage of ED. Attempt is also made on searching for the optimum operating conditions.

Experimental

LTVC concentrated brine of salinity about 15%, which is prepared from RO concentrated brine of salinity about 6% operated at 60°C and 630 mmHg gauge, is used to prepare highly concentrated mineral source water. The RO-concentrated brine is prepared from DSW of salinity about 3.5% drawn at a depth of 618 meters in the coastal area of Hualien County, using UF and RO processes. Typical concentrations of the major ionic species in DSW, RO-concentrated brine, and LTVC concentrated brine are summarized in Table 1.

ED apparatus and electrodialyzer

Referring to Figure 1a, ED is carried out in a laboratory-scaled apparatus (CH-O type Electrodialyzer, Asahi Glass Engineering), which comprises four units for the circulation of the dilute liquid (in tank D), the concentrate liquid (in tank C), the electrode liquid (in tank E), and the interception liquid (in tank I), each is circulated by a circulating pump and passes through the electrodialyzer. The circulation plays the role of a stirrer in a batch stirred tank, which makes the liquid inside well mixed. The volume of the liquid in each tank, including the liquid in the piping and the electrodialyzer, is 3 L initially. Tanks D and C are filled with LTVC concentrated brine and RO pure water, respectively. The electrodialyzer comprises mainly four parts, namely, the

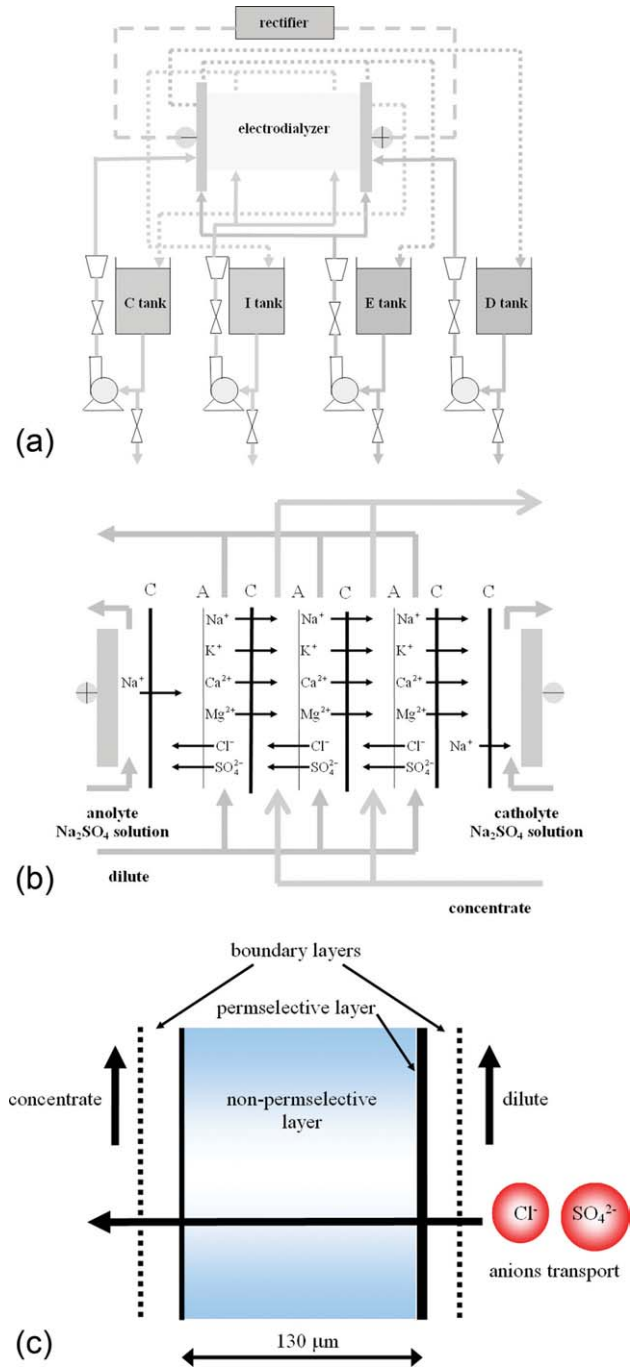

Figure 1. Schematic representation of the ED apparatus adopted.

a: ED apparatus. **b**: Transport of ionic species inside the electrodialyzer. **c**: Selemion ASV anion-exchange membrane. Solid and dashed lines in (a) denote the influx and the efflux, respectively. [Color figure can be viewed in the online issue, which is available at wileyonlinelibrary.com.]

membrane stack, the electrodes, the cell chambers, and the interception chambers. The membrane stack includes 11 cation-exchange membranes and 10 anion-exchange membranes. These membranes are stacked alternately with the outside two being cation-exchange membrane. The cell chambers are filled with circulating electrode liquid, a 4% $NaSO_4$ solution. The interception chambers between the membrane stack and the cell chambers are filled with circulating interception liquid, a 3.5% NaCl solution, and two Selemion CMT cation-exchange membranes are inserted separately at the interfaces between the interception chambers and the cell chambers. On the anode side, the inserted cation-exchange membrane can prohibit the formation of Cl_2 arising from the penetrated Cl^- in the anode chamber. On the cathode side, it can prevent the formation of the scale coming from the penetrated Mg^{2+} and Ca^{2+} in the cathode chamber. A constant DC voltage is applied to the membrane stack through a DC power supply (rectifier) connected to the electrodes. The applied DC voltage and the corresponding current can be read directly from the DC power supply. Figure 1b illustrates the transport of ionic species in the electrodialyzer. After the DC voltage is applied the cations in the dilute chamber migrate toward the cathode, across the cation-exchange membrane (denoted by C), and into the concentrate chamber, where they are blocked by the next anion-exchange membrane (denoted by A) and stay in that chamber. Similarly, the anions in the dilute chamber migrate toward the anode, across the anion-exchange membrane and into the concentrate chamber, where they are blocked by the next cation-exchange membrane and stay in that chamber. Based on these mechanisms, the pure and the highly concentrated mineral source water can be obtained through ED. Our goal is to reduce significantly the content of SO_4^{2-} in the produced mineral source water. To this end, Selemion CMV cation-exchange membrane (standard) and Selemion ASV anion-exchange membrane (monovalent anion permselective) are used in the membrane stack. The former has a resistance of 3 Ω cm^2 for 0.5 M NaCl, and a transfer number of Na^+ larger than 0.96. The latter has a transfer number of Cl^- larger than 0.97, and a resistance of 3.2 Ω cm^2 for 0.5 M NaCl and 13 Ω cm^2 for 0.5 M Na_2SO_4, respectively. Note that while the resistance of Selemion ASV anion-exchange membrane for 0.5 M NaCl is close to that of the standard membrane, its resistance for 0.5 M Na_2SO_4 is several times that for 0.5 M NaCl. As shown in Figure 1c, the significant difference in the resistance of Selemion ASV membrane for Cl^- and that for SO_4^{2-} is achieved mainly by coating a steric-repulsion permselective polymer layer on its surface. The function of this polymer layer will be elaborated later. Table 2 summarizes the specifications of the ED apparatus adopted.

Experimental design

The experimental procedure is illustrated in Figure 2. Tanks C and D are filled with LTVC concentrated brine and RO pure water, respectively, up to 3 L. ED is operated at a prespecified constant DC voltage and a circulation flow rate of 100 L/h. The temperature of the liquid, the electrical current, and the volume of the liquid in tanks C and D are recorded at every 30 min. To estimate both the concentrations of Cl^- and SO_4^{2-}, 50 mL of liquid sample is taken from tank C. Some of the liquid sample is taken and diluted properly with RO pure water; the extent of dilution depends upon the estimated concentration of Cl^-. A yellow $NH_4Fe(SO_4)_2$ solution and a colorless $Hg(SCN)_2$ solution are

Table 2. Specifications of the ED Apparatus Adopted

Number of membranes	20 (10 pairs)
Cation-exchange membrane	Selemion CMV (Asahi Glass Engineering)
Anion-exchange membrane	Selemion ASV (Asahi Glass Engineering)
Effective area of membrane	0.021 m^2 (12 × 17.5 cm^2)
Space between membranes	0.75 mm
Anode	Ti/Pt
Cathode	SUS316
Storage tank: tank C (concentrate)	3.5 L
Tank D (dilute)	3.5 L
Circulating pump	Magnet Pump MD-30R-N (Iwaki)
Flow meter	Area type
DC voltage power supply (rectifier)	PAK35-10A (Kikusui America)
Thermometer	Alcohol-in-glass thermometer

then introduced into the diluted sample. After the addition of these two reagents, the color of the sample turns into orange-red because of the presence of unreacted $NH_4Fe(SO_4)_2$ and the brick-red product, $Fe(SCN)_3$ complex. Then, the concentration of Cl^- is estimated through spectrophotometer measurement (CE9200, Cecil Instruments) using a calibration curve. The chemical reactions involved in these steps can be expressed as

$$Hg(SCN)_2 + 2Cl^- \rightarrow HgCl_2 + 2SCN^- \quad (1)$$

$$3SCN^- + Fe^{3+} \rightarrow Fe(SCN)_3 \quad (2)$$

Note that the amount of $Fe(SCN)_3$ formed is proportional to the amount of Cl^-, the concentration of which can be measured by the procedure above. To determine the concentration of SO_4^{2-}, some of the liquid sample is first diluted properly by RO pure water, followed by the addition of solid $BaCl_2$. Because of the presence of $BaSO_4$ precipitation, the addition of the reagent yields a white turbid dispersion. The concentration of SO_4^{2-} can be estimated through spectrophotometer measurement using a calibration curve. The operation time of ED is set at 300 min and five DC voltage levels are chosen, namely, 5, 7.5, 10, 12.5, and 15 V.

Results and Discussion

Because of the heat generated by the circulating pump, the temperature of the liquid in each tank increases slightly with the operating temperature ranging from 22.5 to 30°C during ED. Because this variation in the temperature is not too large its effect is neglected in subsequent analyses. The experimental data recorded, including the temporal variations in the electrical current, I_a, the liquid volume in tank D, V_d (including the liquid in the piping and the electrodialyzer), the liquid volume in tank C, V_c (including the liquid in the piping and the electrodialyzer), the concentration of Cl^- in tank C, c_{cc}, and the concentration of SO_4^{2-} in tank C, c_{sc}, are summarized in Table 3. Because the initial values of c_{cc} and c_{sc} are zero, they are not listed in Table 3. In contrast, the initial concentrations of Cl^- and SO_4^{2-} in tank D, c_{cd} and c_{sd}, respectively, are included.

Figure 3a illustrates the temporal variations in the electrical current I_a under various levels of V_a. As seen in Figure 3a, if V_a is lower than 7.5 V, I_a increases slowly with time and reaches a constant value at about 60 min. On the other hand, if V_a exceeds 10 V, I_a increases rapidly with time, reaches a maximum value at about 60 min, and then decreases with a further increase in time. The higher the level of V_a the shorter is the time at which I_a begins to decrease. It is interesting to note that for the cases where V_a is 12.5 and 15 V, I_a approaches zero at the final stage of ED. The temporal behavior of I_a seen in Figure 3a reflects the general nature of the ionic transport in ED. The initial ascending of I_a comes mainly from the resistance of the ion-exchange membranes; the larger this resistance the longer the ascending period. This is justified by that the ascending period of each I_a curve is roughly the same, regardless of the level of V_a. If V_a is low, the corresponding rate of ionic transport is slow, and it keeps at a low level after the ascending stage till the end of ED, where that rate is still appreciable. On the other hand, if V_a is high, because the corresponding rate of ionic transport is fast, the ionic transport may become complete before the end of ED. The total amount of ionic species transported can be calculated by integrating I_a with respect to the operation time.

The consumption of the electrical energy, E_a, can be evaluated by

$$E_a(t) = \int_0^t V_a I_a(t)dt = V_a \int_0^t I_a(t)dt \quad (3)$$

Figure 3b shows the temporal variation of E_a for the case of Figure 3a. Figure 3b shows that if V_a is low, E_a increases slowly and roughly linearly with time. On the other hand, if it is high, then E_a increases rapidly and roughly linearly with time in the initial stage, and approaches a constant value toward the end of ED. For a given V_a, Eq. (3) suggests that E_a is the accumulated electric current, and therefore, E_a is proportional to the amount of ionic species transported. The

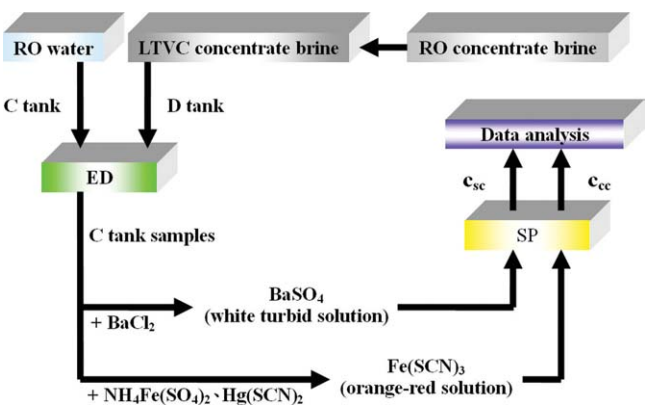

Figure 2. Schematic representation of the experimental procedure.

[Color figure can be viewed in the online issue, which is available at wileyonlinelibrary.com.]

Table 3. Temporal variations in I_a, V_c, V_d, c_{cc}, and c_{sc} at various levels of V_a

		t (min)										
	V_a (V)	0	30	60	90	120	150	180	210	240	270	300
I_a(A)	5	0	1.01	1.63	1.68	1.65	1.61	1.55	1.49	1.44	1.39	1.34
	7.5	0	2.06	3.11	3.21	3.20	3.10	3.03	2.93	2.82	2.73	2.64
	10	0	4.61	5.20	5.23	5.16	4.95	4.68	4.36	3.88	2.93	1.99
	12.5	0	5.63	6.71	6.83	6.65	6.30	5.69	4.04	1.78	0.34	0.18
	15	0	7.16	8.69	8.52	8.14	7.07	3.45	0.85	0.26	0.18	0.16
V_c(L)	5	3.000	2.889	2.805	2.749	2.666	2.624	2.568	2.513	2.499	2.457	2.401
	7.5	3.000	2.903	2.861	2.833	2.833	2.833	2.833	2.847	2.861	2.903	2.903
	10	3.000	2.889	2.903	2.958	2.986	3.056	3.111	3.195	3.279	3.362	3.390
	12.5	3.000	3.014	3.084	3.153	3.251	3.376	3.487	3.571	3.585	3.571	3.571
	15	3.000	2.986	3.098	3.251	3.446	3.599	3.654	3.654	3.641	3.641	3.627
V_d(L)	5	3.000	3.070	3.084	3.084	3.098	3.111	3.125	3.125	3.084	3.084	3.014
	7.5	3.000	3.028	3.000	2.986	2.930	2.875	2.805	2.735	2.652	2.568	2.457
	10	3.000	3.000	2.958	2.861	2.735	2.610	2.471	2.332	2.206	2.081	1.956
	12.5	3.000	2.958	2.847	2.708	2.554	2.346	2.179	2.053	2.039	1.928	1.830
	15	3.000	2.944	2.763	2.541	2.304	2.081	1.956	1.886	1.858	1.817	1.705
c_{cc}(mg/L) (c_{cd} at $t = 0$)	5	87705	705	4467	8645	12972	16772	22504	26835	29510	35242	37917
	7.5	89761	1985	8366	16205	23911	31048	37175	49879	50474	55148	61085
	10	92240	6718	17737	29482	39519	50839	58867	66723	69262	74086	73451
	12.5	90241	7381	20569	36082	48261	59180	67709	72165	73056	69619	67709
	15	91132	9239	27235	43830	59307	69746	71783	70510	69619	68855	67964
c_{sc}(mg/L) (c_{sd} at $t = 0$)	5	10576	34	51	56	58	61	64	67	66	70	71
	7.5	10269	35	60	59	64	64	68	67	77	79	90
	10	10422	64	64	67	67	74	83	111	222	1189	4857
	12.5	10405	218	214	218	216	229	316	1904	6951	7803	8011
	15	10330	113	112	115	127	264	4123	7567	7563	7615	7563

behaviors of E_a seen in Figure 3b can be explained by the corresponding behaviors of I_a illustrated in Figure 3a.

Figure 4 shows the temporal variations of the liquid volume in tanks C and D, V_c and V_d, respectively, at various levels of V_a, where the liquid volume includes that in the piping and that in the electrodialyzer. Because of the sampling of 50 mL of liquid from tank C at each sampling time, the temporal curve of V_c shows a sudden drop at the corresponding time. In addition, because 50 mL of liquid is taken from tank D at the end of ED for checking the total amount of ionic species, the temporal curve of V_d also drops at the corresponding time. As seen in Figure 4, the variations of V_c and V_d are quite interesting. Note that due to the flow of ionic species and water, the liquid volume varies with time. In the LTVC concentrated brine, the mass fraction of ionic species is about 15%, and therefore, the variation in the liquid volume because of the ionic flow is appreciable. The flow of water arises from the effects of electroosmosis and osmosis. The former is caused by the drag force coming from the ionic flow, and the latter by the difference in the solute concentration of the dilute and that of the concentrate. The flow of ionic species and that of water coming from electroosmosis depend mainly on the ionic flux; both of them increase with increasing ionic flux. Because of the presence of the effects of electroosmosis and osmosis, V_d decreases and V_c increases. In the initial stage of ED, because the difference between the solute concentrations in the liquids of tanks C and D is large, the effect of osmosis is significant, and therefore, V_d increases and V_c decreases. The results seen in Figure 4 arise from the competition of the effects of ionic flow, electroosmosis, and osmosis during ED. If V_a is low (5 V), the effects of ionic flow and electroosmosis are insignificant, and therefore, V_d increases and V_c decreases slightly (taking account of the volume decrement due to sampling) with time. As V_a increases to 7.5 V, because those two effects become important, V_d begins to decrease and V_c begins to increase during the mid-stage of ED. If V_a is sufficiently high, then because those two effects

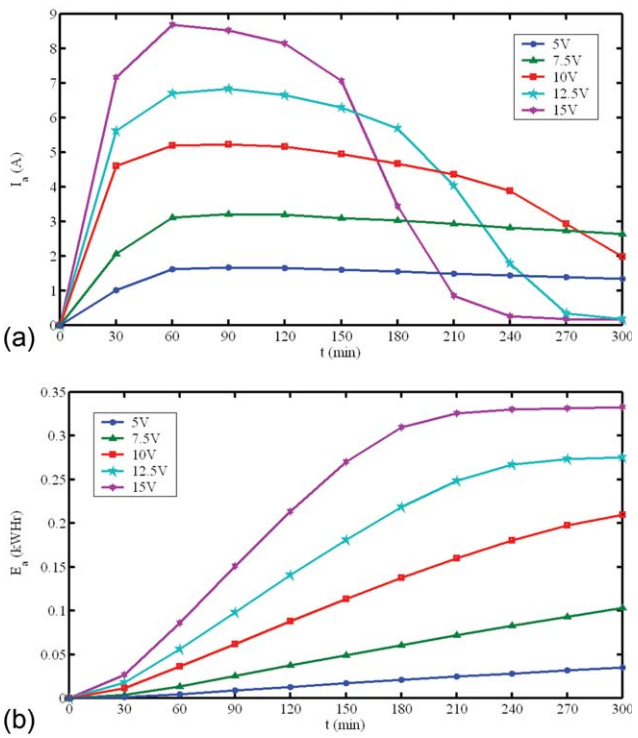

Figure 3. Temporal variation of I_a, (a), and E_a, (b), at various levels of V_a.

Discrete symbols denote the experimental data. [Color figure can be viewed in the online issue, which is available at wileyonlinelibrary.com.]

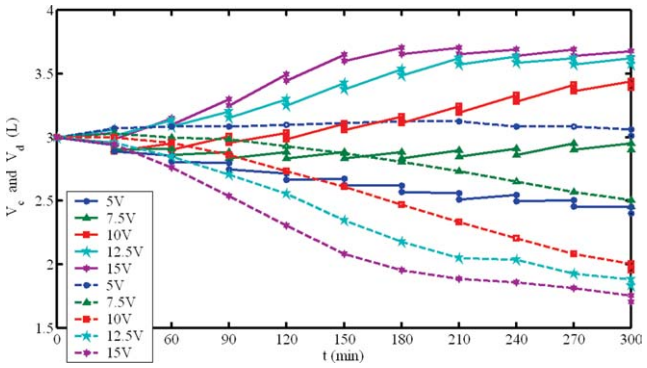

Figure 4. Temporal variations of V_c (solid curves) and V_d (dash curves) at various levels of V_a.

Discrete symbols denote the experimental data. [Color figure can be viewed in the online issue, which is available at wileyonlinelibrary.com.]

dominate V_d decreases and V_c increases appreciably with time.

The separation efficiency of the anion-exchange membrane used can be measured by the total amount (mass) of Cl^- and SO_4^{2-} in tank C, m_{cc} and m_{sc}, respectively. These two values can be evaluated from the liquid volume of tank C, V_c, and c_{cc} and c_{sc}. In the present case, the values of m_{cc} and m_{sc} at each sampling time t_n, $m_{cc}(t_n)$, and $m_{sc}(t_n)$, respectively, can be expressed as

$$m_{cc}(t_n) = c_{cc}(t_n)V_c(t_n) + \sum_{i=1}^{n} 0.05c_{cc}(t_i) \tag{4}$$

and

$$m_{sc}(t_n) = c_{sc}(t_n)V_c(t_n) + \sum_{i=1}^{n} 0.05c_{sc}(t_i) \tag{5}$$

Here, t_i denotes the i-th sampling time. Figure 5 shows the temporal variations of m_{cc} and m_{sc} at various levels of V_a. As seen in Figure 5a, if V_a is low, m_{cc} varies roughly linearly with the operation time t. However, if V_a exceeds 10 V, m_{cc} increases roughly linearly with t in the initial period of ED and then reaches a plateau value at a certain characteristic time, which depends upon the level of V_a; the higher the V_a the shorter the characteristic time is. In general, the higher the level of V_a, the faster is the rate of Cl^- transported. If V_a exceeds 10 V, the transport of Cl^- is complete before the end of ED. Figure 5b shows that the transport behavior of SO_4^{2-} is quite different from that of Cl^- in which the amount of SO_4^{2-} transported is inappreciable during ED for the case where V_a is lower than 7.5 V. If V_a exceeds 10 V, then the amount of SO_4^{2-} transported begins to increase appreciably at a certain characteristic time, which is close to the characteristic time at which m_{cc} reaches a plateau value. Figure 5b also shows that if V_a exceeds 12.5 V, then the total amount of SO_4^{2-} transported reaches a plateau value at the end of ED. To explain the specific transport behavior of SO_4^{2-}, we define the mass fractions of Cl^- and SO_4^{2-} transported to tank C, m_{ccr} and m_{scr}, respectively, as $m_{ccr} = m_{cc}/m_{cd}(0)$ and $m_{scr} = m_{sc}/m_{sd}(0)$, where m_{cd} and m_{sd} are the total amount (mass) of Cl^- and SO_4^{2-} in tank D. Figure 6 illustrates the temporal variations of m_{ccr}, m_{scr}, and $m_{ccr}/(m_{ccr} + m_{scr})$. Note that some of the m_{ccr} values at higher levels of V_a are larger slightly than unity, which arises mainly from the experimental error in measuring the concentration of Cl^-. As seen in Figure 6a, if V_a is lower than 7.5 V, the transport of Cl^- is incomplete at the end of ED, but that of SO_4^{2-} is almost null. However, if V_a exceeds 10 V, while the transport of Cl^- is ongoing before the characteristic time, that of SO_4^{2-} is inappreciable. When the characteristic time is reached, the transport of Cl^- is almost complete and that of SO_4^{2-} starts to become significant; if V_a exceeds 12.5 V, the transport of SO_4^{2-} is almost complete near the end of ED. Figure 6a suggests that the transport of SO_4^{2-} becomes appreciable only when the transport of Cl^- is almost complete. This is why the transport of SO_4^{2-} is negligible during ED for lower levels of V_a. Figure 6b shows that for the case where V_a exceeds 10 V, $m_{ccr}/(m_{ccr} + m_{scr})$ begins to decrease at the characteristic time where the transport of SO_4^{2-} becomes appreciable. The interesting result observed in Figure 6 has not been reported previously in relevant ED experiments. The blocking of the transport of SO_4^{2-} by Cl^- almost completely during ED is unexpected. The monovalent anion permselectivity of Selemion ASV membrane comes from the coating of a highly crosslinked resin on its surface, the permselective layer, which functions as a steric-repulsion barrier because its pores are smaller

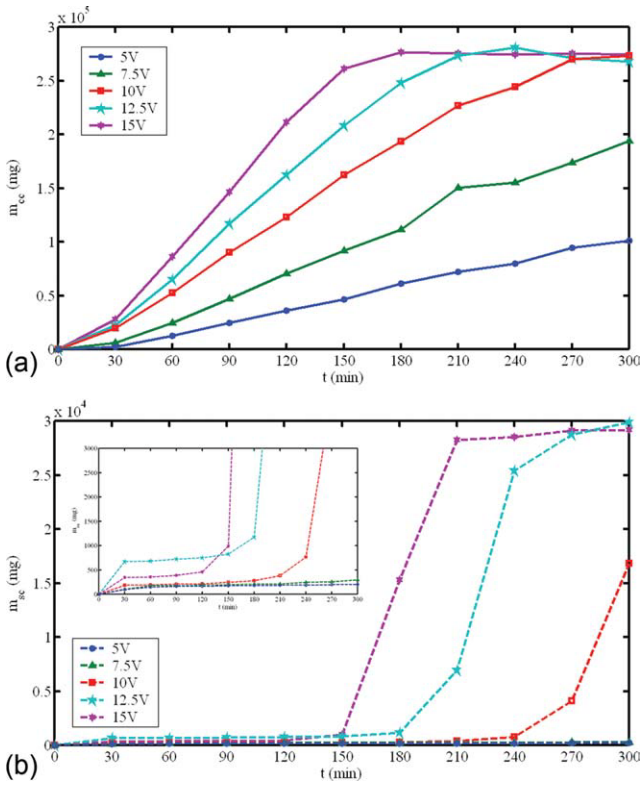

Figure 5. Temporal variations of m_{cc}, (a), and m_{sc}, (b), at various levels of V_a.

Discrete symbols denote the experimental data. [Color figure can be viewed in the online issue, which is available at wileyonlinelibrary.com.]

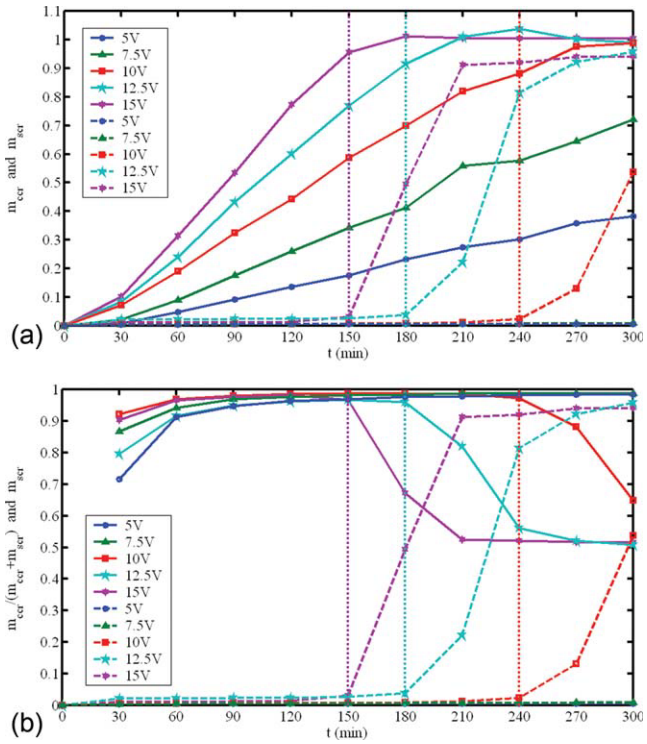

Figure 6. Temporal variations of m_{ccr} (solid curves) and m_{scr} (dash curves), (a), and $m_{ccr}/(m_{ccr} + m_{scr})$ (solid curves) and m_{scr} (dash curves), (b), at various levels of V_a.

Discrete symbols denote the experimental data. Dotted lines represent the characteristic time at which the transport of Cl^- is almost complete and that of SO_4^{2-} begins to increase appreciably. [Color figure can be viewed in the online issue, which is available at wileyonlinelibrary.com.]

than those of the nonpermselective layer. The pore size of the permselective layer is of the order of the size of anions (ca. several Å), and the smaller the anions the easier for them to pass through this layer. The results presented in Figure 6, however, cannot be explained simply by the steric-repulsion mechanism because the transport of SO_4^{2-} is almost totally blocked by Cl^- during ED. The effective radius of Cl^- is 1.81 Å,[15] and the effective radius of SO_4^{2-} estimated from its partial molar volume is 2.33 Å.[16] The difference between these two radii is smaller than 30%. If the pore size of the permselective layer is not very close to the sizes of SO_4^{2-} and Cl^-, the rates of transport of these anions will not differ much because the mobilities of them are close to each other.[17] This implies that if the transport of anions is dominated solely by the steric-repulsion mechanism, the pore size of the permselective layer should be very close to the size of SO_4^{2-}. Figure 7 illustrates the proposed mechanism for the transport of anions through the permselective layer. For simplicity, we consider a two-dimensional problem and assume that the pores on the surface of the permselective layer have the same size and distributed uniformly. To an anion driven by the applied electrical field to the surface of the permselective layer, it is capable of entering the pore only if its projection area on the surface of the permselective layer is smaller than the cross-sectional area of the pore. The probability for an anion to enter the pore is proportional to the areas of these two circle shadows (as are labeled with c on the right-hand side). If we define

$$p_{cs} = \frac{(r_p - r_c)^2}{(r_p - r_s)^2} = \frac{[r_p - (r_s - \Delta r)]^2}{(r_p - r_s)^2} = \frac{[(r_p - r_s) + \Delta r)]^2}{(r_p - r_s)^2} = \left[1 + \frac{\Delta r}{r_p - r_s}\right]^2 \quad (6)$$

where r_p, r_c, and r_s are the radii of the pore, Cl^-, and SO_4^{2-}, respectively, and $\Delta r = (r_s - r_c)$, then p_{cs} is a measure for the ratio (probability for a Cl^- to enter the pore/probability for a SO_4^{2-} to enter the pore). According to Eq. 6, because Δr is constant, if the size of the pore is closer to that of SO_4^{2-}, the probability for a Cl^- to enter the pore is larger than that for a

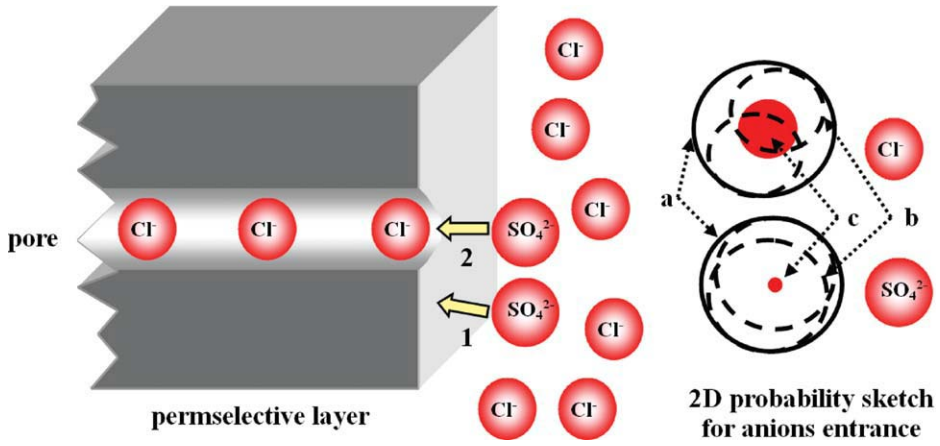

Figure 7. Schematic representation of the proposed mechanism for the transport of Cl^- and SO_4^{2-} through the permselective layer coated on the surface of Selemion ASV anion-exchange membrane.

The solid circle (labeled with a) on the right-hand side denote the inlet of a pore, the dash circle (labeled with b) denotes the projection of an anion on the inlet of the pore, and the shaded circle (labeled with c) denotes the set of centers of projections lying in the inlet of pore. 1 and 2 indicate the two possible orientations of a SO_4^{2-} as it approaches the pore. [Color figure can be viewed in the online issue, which is available at wileyonlinelibrary.com.]

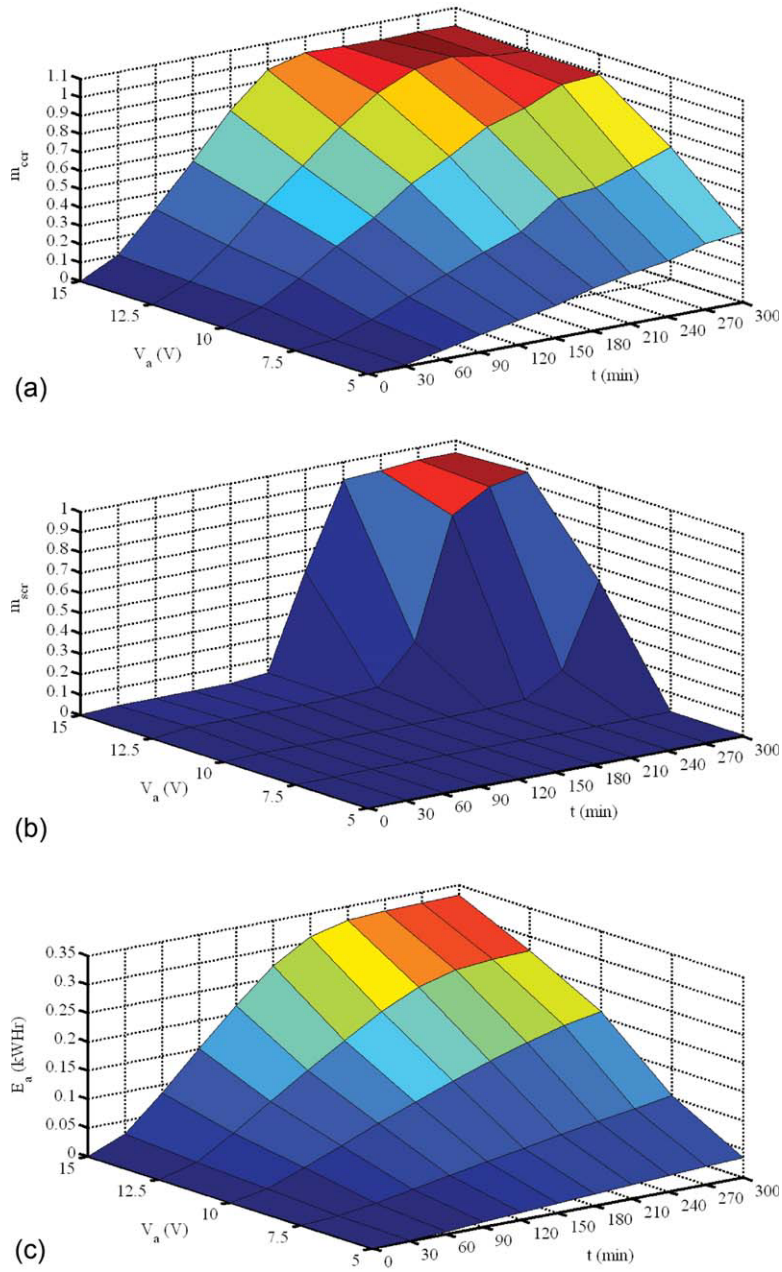

Figure 8. The solution surface of m_{ccr} (a), m_{scr} (b), and E_a, (c), on the $t - V_a$ plane: the grid nodes denote the experimental data.

[Color figure can be viewed in the online issue, which is available at wileyonlinelibrary.com.]

SO_4^{2-}. Depending upon the pore size, p_{cs} can take a very value, that is, the probability for a Cl^- to enter the pore is much larger than that for a SO_4^{2-}. For example, if $r_p = 2.40$ Å, then $p_{cs} \cong 71$, a value large enough for Cl^- to block appreciably the transport of SO_4^{2-} through the permselective layer. In addition, as ED begins, because the transport of Cl^- through the permselective layer dominates, its pores contain mainly Cl^-. In this case, an approaching SO_4^{2-} is either having a projection, which does not lie entirely inside the inlet of a pore (labeled as 1 in Figure 7), or is electrically repelled by the Cl^- already inside the pore (labeled as 2 in Figure 7). Therefore, the probability for the SO_4^{2-} to enter the pore is very small, that is, the transport of SO_4^{2-} through the permselective layer is almost completely blocked by Cl^-.

The discussions above suggest that the performance of the anion-exchange membrane used in reducing the concentration of SO_4^{2-} for the production of mineral source water is satisfactory if ED is operated at the conditions specified by the dot lines in Figure 6. However, to achieve the optimal operation conditions in practice, the consumption of the electrical energy should also be taken into account. Therefore, we define the optimal operation conditions for the present ED are such that the constraints below are satisfied:

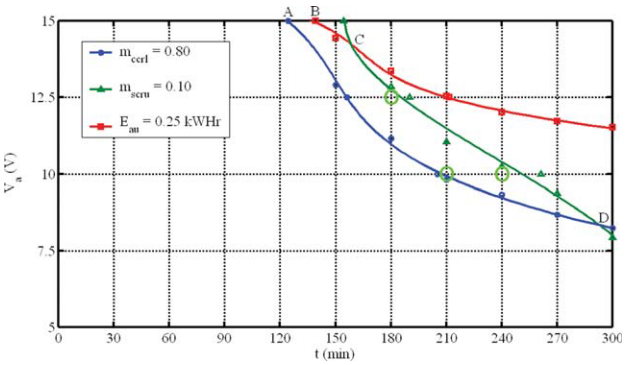

Figure 9. The schematic representation for searching the optimal operation conditions on the $t - V_a$ plane.

The grid nodes denote the experimental data. The irregular region ABCD denotes the domain where the operations satisfy our criteria for optimal operation conditions, and the three circled grid nodes denote the operations in our experiment which lie in this region. The symbols denote the values by interpolation from our experimental data, and the solid curves denote the fitting polynomials of degree three. The values of m_{ccrl}, m_{scru}, and E_{au} for each corresponding curve are indicated on the legend of figure. [Color figure can be viewed in the online issue, which is available at wileyonlinelibrary.com.]

$$m_{\mathrm{ccrl}} \le m_{\mathrm{ccr}} \tag{7}$$

$$m_{\mathrm{scr}} \le m_{\mathrm{scru}} \tag{8}$$

$$E_{\mathrm{a}} \le E_{\mathrm{au}} \tag{9}$$

Here, m_{ccrl} and m_{scru} are the lower bound for m_{ccr} and the upper bound for m_{scr}, respectively, for the mineral source water produced, and E_{au} is a reasonable upper bound for E_a. For example, let us consider the case where $m_{ccrl} = 0.80$, $m_{scru} = 0.10$, and $E_{au} = 0.25$ kWhr. In this case, we search for the intersection curve between the plane $m_{ccrl} = 0.80$ and the solution surface of m_{ccr} over the $t - V_a$ plane shown in Figure 8a that between the plane $m_{scru} = 0.10$ and the solution surface of m_{scr} over the $t - V_a$ plane shown in Figure 8b, and that between the plane $E_{au} = 0.25$ *kWhr* and the solution surface of E_a over the $t - V_a$ plane shown in Figure 8c. The three intersection curves thus obtained are then plotted on the (t, V_a) coordinates shown in Figure 9, where discrete symbols denote the coordinates obtained by interpolating the experimental data gathered and solid curves represent the results of fitting those discrete symbols to polynomials of degree three. The region encircled by these three solid curves, ABCD, represents the possible optimal operation conditions, where the coordinates of A, B, C, and D are (124.2 min, 15 V), (137.3 min, 15 V), (158.2 min, 14.26 V), and (293.1 min, 8.34 V), respectively. The optimal operation conditions of the present ED can be expressed as

$$\begin{aligned}(-0.87201V_{\mathrm{a}}^3 + 34.274V_{\mathrm{a}}^2 - 459.34V_{\mathrm{a}} + 2245.6) \\ \le t \le (0.44273V_{\mathrm{a}}^3 - 13.808V_{\mathrm{a}}^2 + 115.79V_{\mathrm{a}} + 30,901) \\ V_{\mathrm{a}} \in [8.34V, 14.26V]\end{aligned} \tag{10}$$

$$\begin{aligned}(-0.87201V_{\mathrm{a}}^3 + 34.274V_{\mathrm{a}}^2 - 459.34V_{\mathrm{a}} + 2245.6) \\ \le t \le (-5.9227V_{\mathrm{a}}^3 + 247.94V_{\mathrm{a}}^2 - 3479.1V_{\mathrm{a}} + 16526) \\ V_{\mathrm{a}} \in [14.26V, 15V]\end{aligned} \tag{11}$$

In our experiment, three sets of operation conditions, with coordinates (210 min, 10 V), (240 min, 10 V), and (180 min, 12.5 V), circled in Figure 9, satisfy the optimal operation conditions.

Conclusions

A laboratory-scaled ED is adopted to investigate the dependence of the separation efficiency of Cl^- and SO_4^{2-} in the production of mineral source water from DSW on the operating time and the applied DC voltage. Based on the experimental data gathered, we conclude following: (1) After an ascending period of about 60 min, the electrical current (or ionic flux) reaches a lower (higher) plateau for lower (higher) applied DC voltage, and if the applied DC voltage is sufficiently high, the electrical current vanishes before the end of the operation. (2) If the applied DC voltage is high, the change in the liquid volume during ED is dominated by the ionic transport and the effect of electroosmosis. (3) The amount of Cl^- transported varies roughly linearly with the operating time. (4) The transport of SO_4^{2-} during the operation is almost blocked completely by Cl^-, presumably due to that the pore size of the permselective layer is very close to the size of SO_4^{2-}. (5) Based on the constraints of high Cl^- output, low SO_4^{2-} content, and low electrical energy consumption, a region representing the possible optimal operation conditions for the present ED is constructed.

Acknowledgments

This work is financially supported by the Stone & Resource Industry R&D Center and the Ministry of Economic Affairs of the Republic of China. The experimental apparatus, laboratory, and consultation provided by the former are deeply appreciated. Moreover, the authors also thank Miss Wan-Ting Weng for her assistance in the preparation of artworks.

Notation

c_{cc} = concentration of Cl^- in tank C (mg/L)
c_{cd} = concentration of Cl^- in tank D (mg/L)
c_{sc} = concentration of SO_4^{2-} in tank C (mg/L)
c_{sd} = concentration of SO_4^{2-} in tank D (mg/L)
E_a = electrical energy consumption (kWhr)
E_{au} = upper bound of E_a (kWhr)
I_a = electrical current (A)
m_{cc} = total mass of Cl^- in tank C (mg)
m_{ccr} = mass fraction of Cl^- transported to tank C (−)
m_{ccrl} = lower bound of m_{ccr} (−)
m_{cd} = total mass of Cl^- in tank D (mg)
m_{sc} = total mass of SO_4^{2-} in tank C (mg)
m_{scr} = mass fraction of SO_4^{2-} transported to tank C (−)
m_{scru} = upper bound of m_{scr} (−)
m_{sd} = total mass of SO_4^{2-} in tank D (mg)
p_{cs} = a measure for the ratio (probability for a Cl^- to enter the pore/probability for a SO_4^{2-} to enter the pore) defined in Eq. 6
t = operation time of ED (min)
t_i = i-th time interval (min)
V_a = applied DC voltage (Volt)
V_c = volume of liquid in tank C (L)
V_d = volume of liquid in tank D (L)

Literature Cited

1. Saracco G. Ion transport through monovalent-anion-permselective membranes. *Ind Eng Chem Res.* 1994;33:96–101.
2. Saracco G. Transport properties of monovalent-ion-selective membranes. *Chem Eng Sci.* 1997;52:3019–3031.
3. Kabay N, Arda M, Kurucaovali I, Ersoz E, Kahveci H, Can M, Dal S, Kopuzlu S, Haner M, Demircioglu M, Yuksel M. Effect of feed characteristics on the separation performances of monovalent and divalent salts by electrodialysis. *Desalination.* 2003;158:95–100.
4. Van der Bruggen B, Koninckx A, Vandecasteele C. Separation of monovalent and divalent ions from aqueous solution by electrodialysis and nonofiltration. *Water Res.* 2004;38:1347–1353.
5. Kabay N, Kahveci H, Ipek O, Yuksel M. Separation of monovalent and divalent ions from ternary mixtures by electrodialysis. *Desalination.* 2006;198:74–83.
6. Gohil GS, Binsu VV, Shahi VK. Preparation and characterization of mono-valent ion selective polypyrrole composite ion-exchange membranes. *J Membr Sci.* 2006;280:210–218.
7. Bassignana IC, Reiss H. Nonequilibrium effects due to ion transport at the forward biased interface between an electrolyte solution and an infinitely thick ion-exchange membrane. *J Phys Chem.* 1983;87:136–149.
8. Manzanares JA, Murphy WD, Mafe S, Reiss H. Numerical simulation of the nonequilibrium diffuse double layer in ion-exchange membranes. *J Phys Chem.* 1993;97:8524–8530.
9. Hsu JP, Liu BT. Current efficiency of ion-selective membranes: effects of local electroneutrality and Donna equilibrium. *J Phys Chem B.* 1997;101:7928–7932.
10. Rosenberg NW, Tirrell CE. Limiting currents in membrane cells. *Ind Eng Chem.* 1957;49:780–784.
11. Partridge SM, Peers AM. Electrodialysis using ion-exchange membrane. I. Factors limiting the degree of desalting. *J Appl Chem.* 1958;8:49–59.
12. Bobreshova OV, Kulintsov PJ. Non-equilibrium processes in the concentration-polarization layers at the membrane/solution interface. *J Membr Sci.* 1990;48:221–230.
13. Bobreshova OV, Kulintsov PJ, Balavadze EM. Electromembrane systems in conditions of concentration polarization: new developments in the rotating membrane disk method. *J Membr Sci.* 1995;101:1–12.
14. Sata T. Properties of a cation-exchange membrane adsorbed or ion-exchanged with hexadecylpyridinium chloride. *Electrochim Acta.* 1973;18:199–203.
15. Masterton WL, Hurley CN. *Chemistry: Principles and Reactions: A Core Text*, 5th ed. CA, Belmont: Thomson-Brooks/Cole, 2004.
16. Yokoyama H, Ohta T. Temperature dependence of conductivities and ion-association constants of potassium sulfate in water. *Bull Chem Soc Jpn.* 1989;62:345–347.
17. Maron SH, Lando JB. *Fundamentals of Physical Chemistry*. New York: Macmillan Publishing Co. Inc., 1974.

Manuscript received Mar. 20, 2010, and revision received May 11, 2010.